



1 **Measurement report: Aircraft observations of aerosol and**  
2 **microphysical quantities of stratocumulus in autumn over**  
3 **Guangxi Province, China: Diurnal variation, vertical distribution**  
4 **and aerosol-cloud relationship**

5 Sihan Liu<sup>a</sup>, Honglei Wang<sup>a\*</sup>, Delong Zhao<sup>b\*</sup>, Wei Zhou<sup>b</sup>, Yuanmou Du<sup>b</sup>, Zhengguo Zhang<sup>c</sup>, Peng  
6 Cheng<sup>c</sup>, Tianliang Zhao<sup>a</sup>, Yue Ke<sup>a</sup>, Zihao Wu<sup>a</sup>, Mengyu Huang<sup>b</sup>

7 <sup>a</sup> China Meteorological Administration Aerosol-Cloud and Precipitation Key Laboratory, Nanjing  
8 University of Information Science and Technology, Nanjing 210044, China

9 <sup>b</sup> Beijing Weather Modification Center, Beijing 100089, China

10 <sup>c</sup> Weather Modification Office of Guangxi Zhuang Autonomous Region, Nanning 530022, China

11 \*Corresponding author.

12 *E-mail address:* hongleiwang@nuist.edu.cn (H. Wang) and [zhaodelong@bj.cma.gov.cn](mailto:zhaodelong@bj.cma.gov.cn) (D. Zhao)

13

14 **Abstract:** Aerosols and clouds play important roles in the global climate system, and aerosol-cloud  
15 interactions have a significant impact on the radiation balance, water cycle, and energy cycle of the  
16 earth-atmosphere system. To understand the effect of aerosols on the vertical distribution of  
17 stratocumulus microphysical quantities in southwest China, the daily variation characteristics and  
18 formation mechanism of the vertical profiles of stratocumulus microphysical characteristics in this  
19 region were described by using the data of 9 cloud-crossing aircraft observations over Guangxi from  
20 October 10 to November 3, 2020. The influence of aerosol number concentration on cloud  
21 microphysical quantity was analyzed by combining the source of air mass and individual cases.  
22 Aerosol number concentration ( $N_a$ ) and cloud droplet concentration ( $N_c$ ) both decreased gradually  
23 with the increase of altitude below 1500m, and did not change with the height between 1500 m and  
24 3300 m. The inversion layer at the top of the boundary layer (PBL) hindered the increase in the  
25 cloud droplet particle size. The lower layer of the stratocumulus cloud in Guangxi was mainly small  
26 particle-size cloud droplet (effective diameter of cloud droplet,  $E_d < 15 \mu\text{m}$ ), and the middle and  
27 upper layer cloud droplet was large particle-size cloud droplet ( $E_d > 20 \mu\text{m}$ ). The vertical distribution  
28 of cloud microphysical quantity had apparent diurnal variation. When aerosols in the boundary layer



29 were transported to the upper air (14:00 to 20:00), the number of cloud droplets ( $N_c$ ) in the lower  
30 layer decreased, and the small particle-size cloud droplets ( $E_d < 20 \mu\text{m}$ ) in the middle layer and upper  
31 layer increased. When aerosols were transported to the boundary layer (10:00 to 13:00), the number  
32 of small particle-size cloud droplets in the lower layer of the cloud increased. The characteristics of  
33 cloud microphysical quantity were also affected by the source of air mass and the boundary layer.  
34 Under the influence of land air mass or in the boundary layer, the aerosol number concentration ( $N_a$ )  
35 and  $N_c$  were high, and the cloud droplet number concentration spectrum was unimodal.  $N_a$  and  $N_c$   
36 were low under the influence of marine air mass or above the boundary layer, and the cloud droplet  
37 number concentration spectrum was bimodal. The relationship between stratocumulus and aerosol  
38 in this region is consistent with the Twomey effect.  $E_d$  and  $N_a$  remain negatively correlated in  
39 different liquid water content ranges, and FIE ranged from 0.07 to 0.58.

40 **Key words:** Aerosol; Aircraft observations; Cloud microphysical quantities; Vertical profile; the  
41 boundary layer

## 42 **1.Introduction**

43 Clouds are an essential component of the Earth-atmosphere system, covering over 67% of the  
44 Earth's surface (King et al., 2013), with stratocumulus clouds accounting for approximately 20% of  
45 land and water surfaces (Wood, 2012). They can absorb atmospheric long-wave radiation and  
46 reflecting solar short-wave radiation to influence the radiation budget of the Earth's atmospheric  
47 system (Pyrina et al., 2015; Ramanathan et al., 1989; Zelinka et al., 2014). Additionally, they  
48 participate in the global water cycle through precipitation processes (Betts, 2007; Rosenfeld et al.,  
49 2014). Cloud microphysical characteristics are closely related to the climate effect and precipitation  
50 formation of stratocumulus clouds. Differences in cloud water content, cloud droplet number  
51 concentration and cloud droplet size in different regions will produce different radiative forcing and  
52 precipitation (de Boer et al., 2008; Waliser et al., 2011; Yuan et al., 2008).

53 Aerosols are an important source of cloud condensation nuclei, and thus variations in aerosols  
54 can lead to significant changes in the microscopic characteristics of clouds (Chen et al., 2021; Dusek  
55 et al., 2006; Lance et al., 2004). Twomey(1977) suggested that, with the liquid water path of clouds  
56 remaining constant, an increase of aerosol number concentration ( $N_a$ ) would increase in cloud  
57 droplet number concentration ( $N_c$ ) and a decrease in cloud droplet size, thereby enhancing cloud  
58 albedo. Albrecht(1989) proposed that the decrease of cloud droplet particle size caused by the



59 increase of aerosols would further inhibit the precipitation process of clouds and thus extend the  
60 lifetime of clouds.

61 Currently, aircraft observation, ground-based remote, and satellite remote sensing are the main  
62 observation methods used to study the interaction between aerosol and cloud. Many scholars have  
63 confirmed the Twomey effect through observational data (Ferek et al., 1998; Han et al., 1994;  
64 Kleinman et al., 2012; Koren et al., 2005). Based on radar observation data, Kim et al.(2003) found  
65 that AOD in Oklahoma presents a linear proportional relationship with liquid water path (LWP) on  
66 a completely cloudy day with single-layer clouds, and the effective radius of cloud droplets is  
67 negatively correlated with the surface aerosol light scattering coefficient. For a given LWP, Cloud  
68 albedo and radiative forcing are very sensitive to the effective radius. Li et al.(2019) using aircraft  
69 observation data over the Loess Plateau, found a negative correlation between  $N_a$  and  $N_c$  in both  
70 vertical and horizontal directions. Under high aerosol loading, smaller cloud droplets with higher  
71 droplet number concentration were observed under high aerosol loading, while fewer larger cloud  
72 droplets were formed under low aerosol loading. Cloud droplet number concentration was  
73 negatively correlated with cloud droplet diameter within a certain range of liquid water content.  
74 However, some scholars have also observed a positive correlation between aerosol and effective  
75 diameter of cloud droplets ( $E_d$ ) (Harikishan et al., 2016; Jose et al., 2020; Liu et al., 2020), referred  
76 to as the anti-Twomey effect.

77 Aircraft observations with continuous vertical sampling are the most reliable source that can  
78 accurately characterize the vertical relationship between aerosol and cloud (Nakajima et al., 2005;  
79 Terai et al., 2014; Wehbe et al., 2021; Zaveri et al., 2022). McFarquhar et al.(2021) conducted  
80 aircraft observations in the Southern Ocean region. They found aerosols above clouds may originate  
81 from new particle formation and remote transport from continental air masses. This leads to cloud  
82 condensation nuclei (CCN) variations and droplet concentration near cloud tops. During the ACE-  
83 ENA campaign, the probability of aerosol transport interacting with marine boundary layer clouds  
84 over the eastern North Atlantic (ENA) during summer was approximately 62.5% (Wang et al., 2020).

85 Zhao et al.(2019) observed a stratus cloud (water cloud) in the Huanghua region of China by  
86 aircraft and found that in the planetary boundary layer (PBL) cloud, the effective radius of cloud  
87 droplets and  $N_a$  show a negative relationship, while they show a clear positive relationship in the  
88 upper layer above PBL with much less  $N_a$ . It also shows that the relationship between the effective



89 radius of cloud droplets and Na changes from negative to positive when LWC increases. Lu et  
90 al.(2007) compared the microphysical quantities of stratocumulus clouds influenced by aircraft  
91 flight tracks and those in undisturbed regions, and found that the effective radius of cloud droplets  
92 in the flight path region was smaller, the number concentration of hair drops was lower, and the  
93 cloud LWC was larger, providing observational evidence for the first indirect effect.

94 The mechanism of interaction between aerosols and clouds still involves significant uncertainty,  
95 influenced by factors such as aerosol physicochemical properties, meteorological conditions, cloud  
96 types, and the relative positioning of aerosols and cloud layers (Almeida et al., 2014; Dusek et al.,  
97 2006; Wex et al., 2010; Zhang et al., 2011). Therefore, precise measurements of cloud microphysical  
98 properties are crucial as the first step in studying aerosol-cloud interactions. Multi-aircraft  
99 observations provide high-precision observational data, aiding in understanding the relationship  
100 between aerosols and cloud microphysical characteristics.

101 Our study on the vertical distribution of aerosol in the Guangxi region found that the vertical  
102 profile of Na in this region has prominent diurnal variation characteristics under the influence of the  
103 boundary layer. In the morning, aerosols are mainly concentrated in the boundary layer. With the  
104 development of the boundary layer and the enhancement of turbulent activity, the aerosols near the  
105 ground are diluted in the afternoon, and some of the aerosols will be transmitted to more than 2 km  
106 altitude. At night, the rapid decline of the boundary layer top will increase Na near the surface. At  
107 the same time, some aerosols will stay above the boundary layer top, forming a high-concentration  
108 aerosol layer (Liu et al., 2024). Previous studies have indicated that aerosols can have microphysical  
109 properties of clouds and enhance indirect effects by entrainment into cloud tops when aerosol  
110 particles settle or clouds deepen (Lu et al., 2018; Painemal et al., 2014). This study used data from  
111 nine cloud-penetrating aircraft flights to investigate the vertical distribution and formation  
112 mechanisms of cloud microphysical properties in stratocumulus clouds over the Guangxi region.

113 Additionally, we discussed the differences in the impact of aerosols from different sources on  
114 cloud microphysical properties. We demonstrated that this region's correlation between aerosols and  
115 clouds conforms to the Twomey effect. The ultimate goal is to provide observational constraints for  
116 the simulation of aerosol radiative forcing in global climate models.

## 117 **2. Data and methodology**

### 118 **2.1. Aircraft data and reanalyze data**



119 The Beijing Weather Modification Office (BJWMO) provided the data for this study, and nine  
 120 flights of stratocumulus clouds and aerosols over Guangxi were conducted using the King Air 350  
 121 ER turbo aircraft. The aircraft is equipped with the Aircraft Integrated Meteorological Measurement  
 122 System (AIMS-20, Aven tech Inc., Canada), which provides meteorological elements such as  
 123 temperature (T) and relative humidity (RH) with a time resolution of 1 s. A passive cavity aerosol  
 124 spectrometer probe (PCASP-100X, DMT Inc, USA) was installed to provide aerosol number  
 125 concentrations in the particle size range of 0.11 to 3  $\mu\text{m}$ , with a time resolution of 1s, particle size  
 126 accuracy of 20%, and concentration accuracy of 16%. The Fast Cloud Droplet Probe (FCDP, SPEC  
 127 Inc, USA) was used to observe the cloud droplet concentration, cloud particle concentration and  
 128 cloud particle size distribution. Its principle is to detect particles from 2  $\mu\text{m}$  to 50  $\mu\text{m}$  by using  
 129 forward scattering technology, with a time resolution of 1s. All instruments were calibrated before  
 130 observation. The detailed principles of the airborne instruments can be found in the following  
 131 studies (Collaud Coen et al., 2010; Strapp et al., 1992; Zhang et al., 2009).

132 **Table 1** Flight information for the measurement campaign.

Date	Take-off/landing time(Local time)	Cloud base/cloud top height (m)	Inside cloud Na( $\text{cm}^{-3}$ )	Nc( $\text{cm}^{-3}$ )	LWC( $\text{g}\cdot\text{m}^{-3}$ )	$E_d(\mu\text{m})$
20201010	11:53–15:50	1203-1652	355 (157)	586 (328)	0.45 (0.30)	12.25 (1.92)
20201011	14:26–17:53	1261-1542	636 (290)	529 (350)	0.19 (0.14)	9.45 (1.30)
20201025	09:34–12:58	1076-3298	9 (31)	38 (35)	0.18 (0.15)	26.96 (9.80)
20201026	09:53–13:29	1367-3146	5 (19)	35 (27)	0.10 (0.09)	21.86 (8.77)
20201028	14:05–17:27	1664-2729	239 (229)	354 (502)	0.45 (0.43)	16.90 (9.54)
20201029	10:05–13:33	516-3266	1402 (569)	396 (289)	0.17 (0.16)	9.86 (2.54)
20201101	18:17–22:06	1661-2715	333 (170)	199 (80)	0.35 (0.17)	17.93 (4.71)
20201102	14:04–17:41	696-3145	177 (174)	136 (97)	0.22 (0.15)	17.45 (3.51)
20201103	14:17–17:28	2021-2938	44 (30)	139 (57)	0.29 (0.10)	15.73 (3.56)

133 Detailed data of this aircraft observation activity, including observation date, time, cloud  
 134 thickness and microphysical quantities, are summarized in Table 1. Compared with aircraft  
 135 observation data in other regions, the average liquid water content (LWC) in Guangxi was higher,  
 136 5.33 times that in North China, and the average cloud droplet diameter was larger, 2.58 times that



137 in North China (Zhao et al., 2011). Compared with Marine Stratocumulus (Lu et al., 2011; Miles et  
138 al., 2000), the stratospheric clouds in Guangxi had higher cloud base height and greater cloud  
139 thickness. The cloud microphysical characteristics of Stratocumulus observed in this study are close  
140 to those of previous observations. Compared with Stratocumulus (non-precipitation warm cloud)  
141 over eastern China, the  $N_c$ , LWC and  $E_d$  of Stratocumulus in Guangxi region were larger. According  
142 to previous studies (Liu et al., 2024), there were no special weather processes in the upper air and  
143 on the ground in Guangxi during the observation period, which ensured the quality of the data and  
144 the universality of the conclusions.

145 The vertical pressure velocity ( $\text{Pa}\cdot\text{s}^{-1}$ ) was obtained from MERRA2, with a spatial resolution  
146 of  $0.625^\circ\times 0.5^\circ$  and 42 layers, and a temporal resolution of 3 hours. The data from the first to the  
147 twenty-third layers, corresponding to pressure altitudes from 1000 hPa to 200 hPa, were selected,  
148 covering the maximum altitude of aircraft observations. An average calculation was performed to  
149 obtain the vertical pressure velocity for the Guangxi region from 8:00 to 20:00 during the  
150 observation period, reflecting the diurnal variation characteristics of vertical airflow above the  
151 region. This dataset has been used in several studies (Ge et al., 2021; Kennedy et al., 2011; Painemal  
152 et al., 2021).

## 153 2.2. Data processing

154 To ensure data quality, this study selected the data that met the following conditions and the  
155 flight macro record as the in-cloud data:  $N_c \geq 10 \text{ cm}^{-3}$ ,  $\text{LWC} \geq 10^{-3} \text{ g m}^{-3}$  (Gunthe et al., 2009;  
156 Zhang et al., 2011). The observation records show that the clouds during the observation period  
157 were stratocumulus clouds (non-precipitation warm clouds). Therefore, this paper's aerosol and  
158 cloud microphysical data met the following conditions: observation height  $\leq 4000 \text{ m}$ ,  $T > 0^\circ\text{C}$ .

159 The microphysical quantities such as  $N_c$ , LWC and  $E_d$  are calculated from the cloud droplet  
160 spectrum data detected by FCDP. The calculation formulas are as follows:

$$161 \quad N_c = \sum n_i \quad (1)$$

$$162 \quad \text{LWC} = \sum \frac{4}{3} \pi r_i^3 \rho_w n_i \quad (2)$$

$$163 \quad E_d = 2 \frac{\sum n_i r_i^3}{\sum n_i r_i^2} \quad (3)$$

164 Define the relative height of the cloud as  $Z_n$



165 
$$Z_n = \frac{Z - Z_{\text{base}}}{Z_{\text{top}} - Z_{\text{base}}} \quad (4)$$

166  $Z_{\text{base}}$  is the height of the cloud base, and  $Z_{\text{top}}$  is the height of the cloud top

167 Similar to previous studies, the first indirect effect or Twomey effect of aerosols and clouds is  
168 defined as

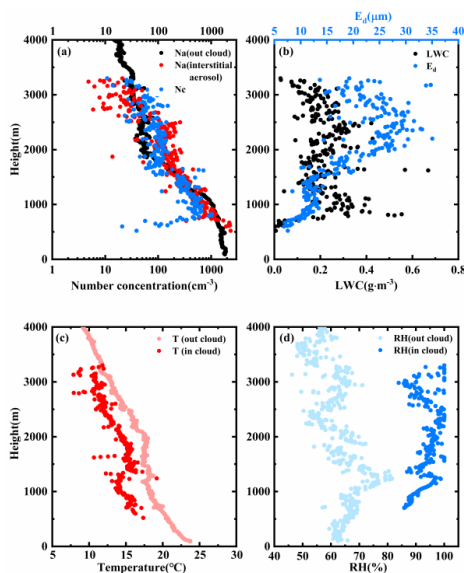
169 
$$\text{FIE} = - \left( \frac{\Delta \ln E_d}{\Delta \ln \alpha} \right)_{\text{LWC}} \quad (5)$$

170 Where is the amount of  $\alpha$  aerosol, which can be used as aerosol optical depth (Feingold et al., 2001),  
171 aerosol extinction coefficient (Feingold et al., 2003), cloud condensation nucleus concentration and  
172 aerosol number concentration (Che et al., 2021; Zhao et al., 2012; Zhao et al., 2018). The value of  
173 FIE may vary with variables representing the amount of aerosol.

### 174 **3. Results and discussion**

#### 175 **3.1 Vertical distribution characteristics of cloud microphysical quantities**

176 The average value of the observation data of 9 sorties was calculated at the interval of 10 m  
177 height, and the average vertical profiles of  $N_a$  (interstitial aerosol),  $N_a$  (out cloud), cloud  
178 microphysical quantity and meteorological elements during the observation period was obtained  
179 (Fig. 1).  $N_a$  (interstitial aerosol) decreased gradually with height, and was affected by aerosols in  
180 atmospheric environment. Below 1500 m,  $N_a$  was high, with an average value of  $749 \text{ cm}^{-3}$ . From  
181 1500 m to 3300 m,  $N_a$  (interstitial aerosol) was low, with an average of  $107 \text{ cm}^{-3}$ .  $N_c$  decreased first  
182 and then remained unchanged with the increase of height. Below 1500 m, there were more cloud  
183 condensation nuclei in the atmosphere,  $N_c$  was high, with an average value of  $407 \text{ cm}^{-3}$ . Between  
184 1500 and 3300 m, the  $N_c$  changed little with the increase of height, and the range of  $N_c$  is 10-200  
185  $\text{cm}^{-3}$  (Fig. 1a).

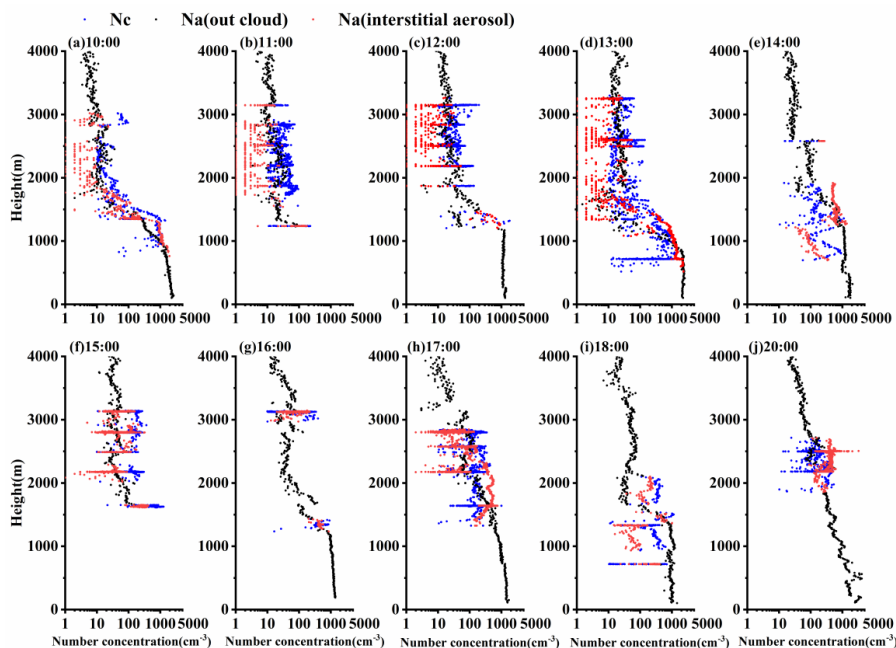


186  
187 **Fig. 1** Average vertical profiles of cloud interstitial aerosol concentration, outside aerosol number concentration,  
188 cloud droplet concentration (a), LWC, effective diameter of cloud droplet (b), temperature inside and outside cloud  
189 (c), and relative humidity inside and outside cloud (d) during the observation period

190 With the increase of height,  $E_d$  first increased, then remained unchanged and then increased  
191 (Fig. 1b). A large number of cloud droplets competed for water vapor below 1500 m, which is not  
192 conducive to the growth of cloud droplets, so the average  $E_d$  was only 11.21  $\mu\text{m}$ . The temperature  
193 inversion layer of 1000-1500 m (Fig. 1c) is an essential factor hindering the growth of cloud droplets.  
194 Above 1500 m,  $N_c$  was lower than the near ground, and the lower atmospheric temperature was  
195 conducive to increasing cloud droplet particle size. The average value of  $E_d$  reached 22.78  $\mu\text{m}$ . The  
196 value of LWC was independent of height, with an average value of 0.22  $\text{g}\cdot\text{m}^{-3}$  in Guangxi (Fig. 1b).

### 197 3.2 Diurnal variation of the vertical distribution of cloud microphysical quantities





198

199

200

201

202

203

204

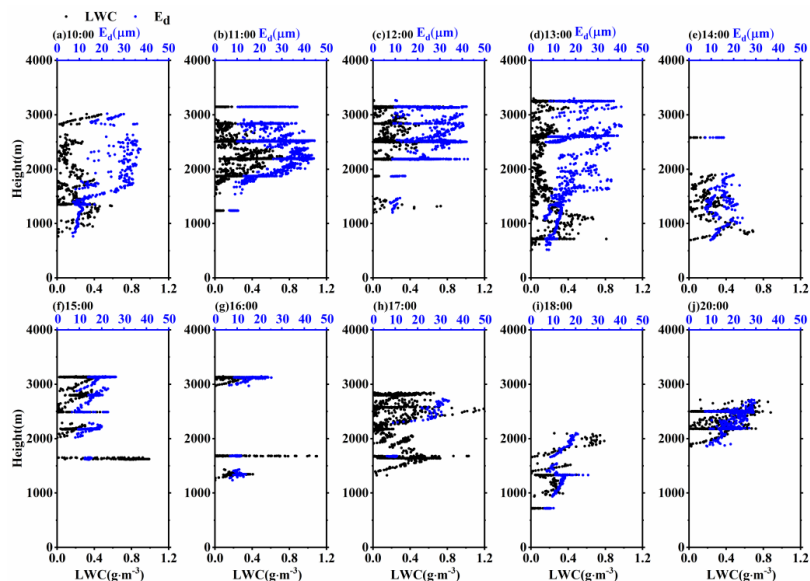
205

206

207

**Fig. 2** Vertical profiles of cloud interstitial aerosol concentration, outside aerosol number concentration, cloud droplet concentration at different times (a is 10:00, b is 11:00, c is 12:00, d is 13:00, e is 14:00, f is 15:00, g is 16:00, h is 17:00, i is 18:00, j is 20:00)

To further understand the diurnal variation of the vertical distribution of cloud microphysical quantities, the data were classified, and the vertical profiles of Na (interstitial aerosol), Na outside the cloud (Fig. 2), cloud microphysical quantities (Fig. 3), and meteorological elements inside and outside the cloud (Fig. 4) at 10 times from 10:00 to 18:00 and 20:00 were obtained. The data in the cloud was the original data, and the average value outside the cloud was calculated at the interval of 10 m.

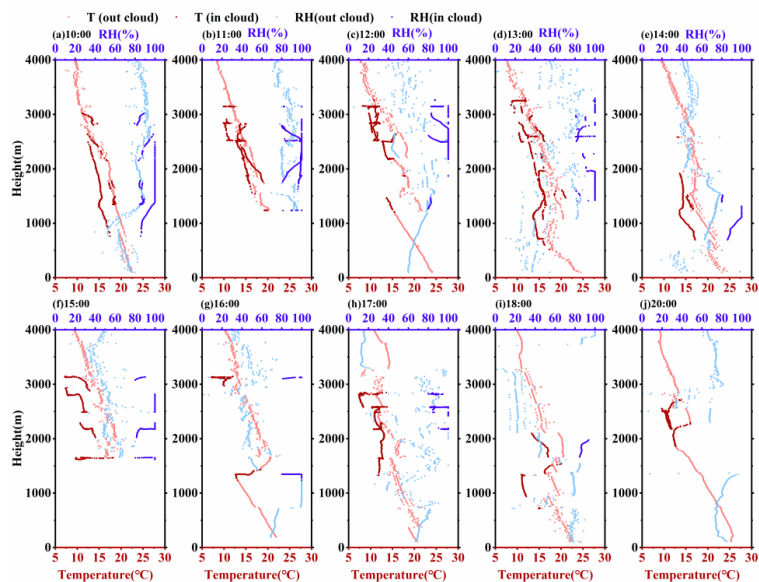


208

209

210

**Fig. 3** Vertical profiles of liquid water content and effective diameter of cloud droplets at different times (a 10:00, b 11:00, c 12:00, d 13:00, e 14:00, f 15:00, g 16:00, h 17:00, i 18:00, j 20:00)



211

212

213

214

215

216

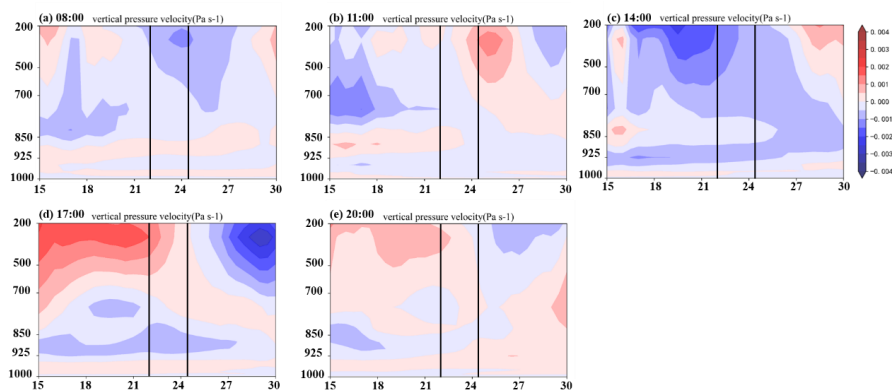
**Fig. 4** Vertical profiles of temperature inside and outside the cloud, relative humidity inside and outside the cloud at different times (a is 10:00, b is 11:00, c is 12:00, d is 13:00, e is 14:00, f is 15:00, g is 16:00, h is 17:00, i is 18:00, j is 20:00)

At 10:00,  $N_c$  below 900 m was less than  $100 \text{ cm}^{-3}$ , and  $N_a$  in PBL was high (Fig. 2a). Although there were sufficient aerosols that can be activated into cloud condensation nuclei, the atmospheric



217 temperature was high, which was not conducive to the activation of aerosol particles (Fig. 4a). At  
218 the same time, LWC was low, and the condensed cloud droplets are difficult to grow, and the average  
219  $E_d$  is only  $8.01 \mu\text{m}$  (Fig. 3a). Between 900m and 1500 m, there were not only sufficient cloud  
220 condensation nuclei, but also sufficient water vapor and temperature conditions, which are  
221 conducive to the formation of cloud droplets. The average  $N_c$  and  $E_d$  increased to  $430 \text{ cm}^{-3}$  and  
222  $11.15 \mu\text{m}$ . Above 1500 m, although the water vapor condition was sufficient, the cloud condensation  
223 nucleus was few, resulting in an average  $N_c$  value of only  $35 \text{ cm}^{-3}$ . However, sufficient LWC was  
224 conducive to the growth of cloud droplets, and  $E_d$  was significantly higher than that of clouds below  
225 1500 m, with  $E_d$  ranging from  $13.82$  to  $37.26 \mu\text{m}$ .  $N_a$  (interstitial aerosol) showed a slight increase  
226 at 1500-1600 m, which may be due to the presence of a temperature inversion layer in the cloud  
227 (Fig 4a), and the entanglement mixing at the cloud base mixed warm air outside the cloud into the  
228 cloud (Lu et al., 2011).

229 At 11:00, more aerosols can activate into cloud condensation nuclei near the top of PBL. The  
230 average  $N_c$  value was  $102 \text{ cm}^{-3}$ , while the average LWC value was only  $0.03 \text{ g}\cdot\text{m}^{-3}$ , cloud droplets  
231 were competing for water vapor, and  $E_d$  was only  $8.20 \mu\text{m}$ , which was similar to the cloud  
232 microphysical characteristics near PBL at 10:00. From 1500 to 3150 m,  $N_a$  was less than  $10 \text{ cm}^{-3}$ ,  
233 the cloud condensation nucleus was insufficient, and the average  $N_c$  was only  $29 \text{ cm}^{-3}$ . Compared  
234 with 10:00, LWC was higher (mean  $0.19 \text{ g}\cdot\text{m}^{-3}$ ), so  $E_d$  in the upper part of the cloud was more  
235 significant, with an average of  $28.95 \mu\text{m}$



236  
237 **Fig 5** Latitudinal profiles of vertical pressure velocity at different times in Guangxi (solid black line is the latitude  
238 range observed by aircraft, positive value is downdraft, negative value is updraft, a is 8:00, b is 11:00, c is 14:00, d  
239 is 17:00, e is 20:00)

240 At 12:00, under the combined action of the uplift of PBL and the updraft (Fig. 5b), the near-



241 surface aerosol was transported to 1200~1500 m (the mean value of  $N_a$  outside the cloud was 578  
242  $\text{cm}^{-3}$ ), the mean value of  $N_c$  reached  $399 \text{ cm}^{-3}$ , and the mean value of  $E_d$  was only  $9.41 \mu\text{m}$ , higher  
243 than 11:00. Stratocumulus clouds above 1800 m have low  $N_c$  (mean  $35 \text{ cm}^{-3}$ ) and large  $E_d$  (mean  
244  $26.14 \mu\text{m}$ ).

245 At 13:00, below 1200m, the range of  $N_c$  was  $13\sim 2052 \text{ cm}^{-3}$ , possibly due to the different  
246 degrees of cloud development at different locations. Compared with 10:00, the updraft speed in  
247 Guangxi at 13:00 increased (Fig. 5b-c), which was conducive to the condensation of cloud droplets.  
248 Therefore,  $N_c$  at 13:00 is more significant than that at 10:00, and many cloud droplets hinder their  
249 particle size growth, with an average  $E_d$  value of  $9.23 \mu\text{m}$ . From 1200 m to 1500 m, the mean values  
250 of  $N_c$  and  $E_d$  were  $155 \text{ cm}^{-3}$  and  $12.29 \mu\text{m}$ . At this height, a strong inversion layer appeared and  
251 cloud droplet evaporation activity was enhanced (Li et al., 2003), resulting in a higher  $N_a$  (interstitial  
252 aerosol) than  $N_a$  (out cloud). For Stratocumulus clouds above 1500 m, the  $N_c$  varied little with  
253 height, and the average  $E_d$  was  $21.45 \mu\text{m}$ .

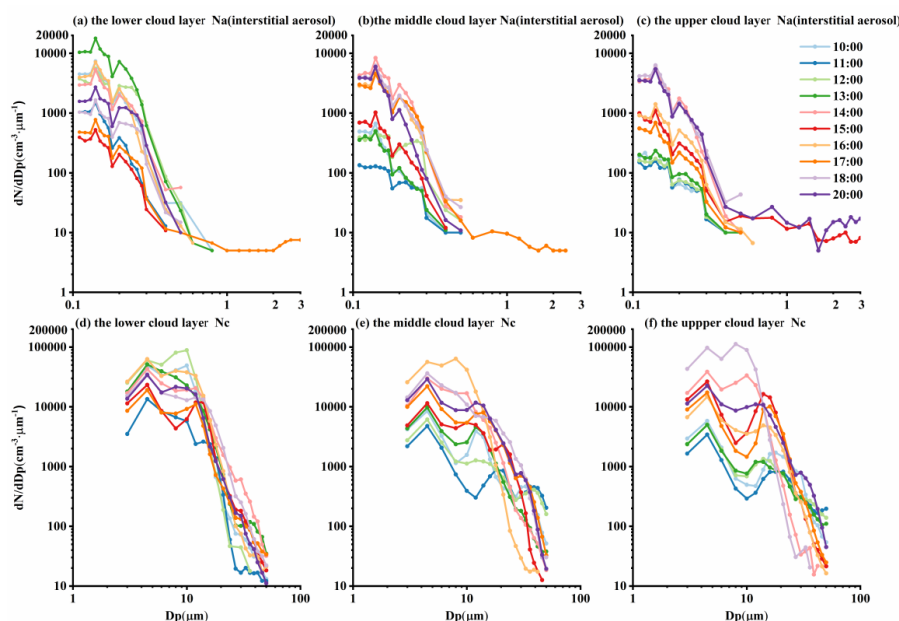
254 At 14:00, the  $N_c$  range below 1500 m was  $11\sim 1109 \text{ cm}^{-3}$ , and the top height of PBL was the  
255 highest, which diluted aerosols in PBL. The average value of LWC was  $0.29 \text{ g}\cdot\text{m}^{-3}$  (Fig. 3e), which  
256 was higher than 13:00, providing water vapor conditions for the growth of cloud droplets. Therefore,  
257 the average value of  $E_d$  reached  $13.75 \mu\text{m}$ . An inversion layer appeared at 2500 m, hindering the  
258 diffusion of aerosols and enhancing the evaporation of cloud droplets near the cloud top, resulting  
259 in the peak of  $N_a$  (interstitial aerosol) at this height.

260 At 15:00, there were more cloud droplets and cloud interstitial aerosol near the top of PBL,  
261 and the average value of  $N_c$  and  $N_a$  (interstitial aerosol) was  $720 \text{ cm}^{-3}$  and  $249 \text{ cm}^{-3}$  (Fig. 2f). The  
262 average value of  $E_d$  was only  $13.72 \mu\text{m}$  due to more cloud droplets. The updraft transports low-level  
263 aerosols upward, increasing the mean value of  $N_c$  above 2000 m to  $146 \text{ cm}^{-3}$ . The mean value of  $E_d$   
264 decreased to  $16.73 \mu\text{m}$  due to the increase of small particle-size cloud droplets.

265 At 16:00,  $N_c$  and  $N_a$  (interstitial aerosol) below 2000 m were relatively large, which were 458  
266 and  $468 \text{ cm}^{-3}$ , respectively. The inversion layer at the top of PBL hinders the condensation growth  
267 of cloud droplets, and the average  $E_d$  was only  $11.00 \mu\text{m}$  (Fig. 3g). Similar to 15:00,  $N_a$  (out cloud)  
268 and  $N_a$  (interstitial aerosol) near 3000 m were higher. Low temperature and high humidity (Fig. 4g)  
269 were conducive to the activation of aerosol, so the maximum value of  $N_c$  reaches  $395 \text{ cm}^{-3}$ , and the  
270 average value of  $E_d$  is only  $17.13 \mu\text{m}$  due to water vapor contention between cloud droplets.



271 At 17:00, the height of the top of PBL decreased, and part of the aerosol remained above PBL,  
272 providing enough cloud condensation nuclei.  $N_c$  did not change with the height (Fig 2h), with an  
273 average value of  $134 \text{ cm}^{-3}$ , and  $E_d$  concentrated in the  $10\text{-}20 \mu\text{m}$  (Fig 3h). Under the cooling of the  
274 atmosphere and the cooling of the cloud tops at sunset, the  $E_d$  near the cloud tops is greater than  $30$   
275  $\mu\text{m}$ . The temperature inversion layer of  $1600\text{-}2000 \text{ m}$  (Fig. 4h) enhanced the growth of cloud  
276 droplets and impeded the diffusion of aerosols, resulting in  $N_a$  (interstitial aerosol) being more  
277 significant than  $N_a$  (out cloud).



278  
279 **Fig 6** Cloud interstitial aerosol number concentration spectrum and cloud droplet number concentration spectrum  
280 (a-c is the aerosol spectrum of lower cloud, middle cloud and upper cloud, and d-f is the cloud droplet spectrum of  
281 lower cloud, middle cloud and upper cloud, respectively)

282 At 18:00, the rapid decline in the top height of PBL resulted in the accumulation of aerosol in  
283 the outer cloud between  $900 \text{ m}$  and  $1400 \text{ m}$  (Fig. 2i), which provided sufficient cloud condensation  
284 nuclei and was conducive to the formation of more small particle-size cloud droplets (the mean  $N_c$   
285 value was  $273 \text{ cm}^{-3}$ , and the mean  $E_d$  value was  $16.67 \mu\text{m}$ ). Similar to 17:00, the atmospheric  
286 ambient temperature above  $1400 \text{ m}$  was high, and cloud droplet evaporation caused  $N_a$  (interstitial  
287 aerosol) to be close to or greater than  $N_a$  (out cloud).

288 At 20:00, the aerosols lingering above the top of PBL spread to the upper air with the updraft,  
289 and sufficient cloud condensation nuclei and low temperature were conducive to the formation and



290 growth of cloud droplets. The mean value of  $N_c$  was  $194 \text{ cm}^{-3}$  respectively (Fig. 2j), which was  
291 much higher than  $N_c$  from 10:00 to 13:00. LWC and  $E_d$  gradually increased with height (Fig. 3j).  
292 LWC increased from  $0.02 \text{ g}\cdot\text{m}^{-3}$  to  $0.64 \text{ g}\cdot\text{m}^{-3}$ , and  $E_d$  increased from  $7.52 \mu\text{m}$  to  $29.59 \mu\text{m}$ .

293 The cloud height is normalized, and the relative height of the cloud is set as  $Z_n$  ( $0 \leq Z_n \leq 1$ ).  
294  $Z_n < 0.33$  is defined as the lower cloud layer,  $0.33 \leq Z_n < 0.67$  is the middle cloud layer, and  $Z_n \geq$   
295  $0.67$  is the upper cloud layer. The concentration spectra of cloud interstitial aerosol numbers (Fig.  
296 6a-c) and cloud droplet numbers (Fig. 6d-f) at different locations at different times were obtained.  
297 The vertical distribution of cloud microphysical quantities of stratocumulus in Guangxi showed  
298 noticeable diurnal variation.

299 From 10:00 to 13:00,  $N_a$  and  $N_c$  in the cloud lower layer were large, cloud droplet diameter  
300 was concentrated below  $20 \mu\text{m}$ , large cloud droplet was less, and  $E_d$  was small.  $N_a$  and  $N_c$  in the  
301 middle cloud layer were less than those in the lower cloud layer.  $N_a$  and  $N_c$  the upper cloud layer  
302 are the smallest. Sufficient water vapor was conducive to the hygroscopic growth of cloud droplets,  
303 so the number of small particle-size cloud droplets in the upper cloud layer was smaller than that in  
304 the middle cloud layer.

305 From 14:00 to 16:00, the updraft diffused aerosols in the lower atmospheric layer upward, and  
306  $N_a$  and  $N_c$  in the lower cloud layer decreased, which was conducive to the condensation growth of  
307 cloud droplets, and the number of cloud droplets with a diameter greater than  $20 \mu\text{m}$  increased. The  
308 upward transport of aerosol causes  $N_a$  and  $N_c$  in the cloud and the upper layer to be larger than  
309 those from 10:00 to 13:00, and newly generated cloud droplets compete for water vapor, resulting  
310 in a decrease in the number of cloud droplets larger than  $30 \mu\text{m}$  in diameter and an increase in small  
311 particle-size cloud droplets.

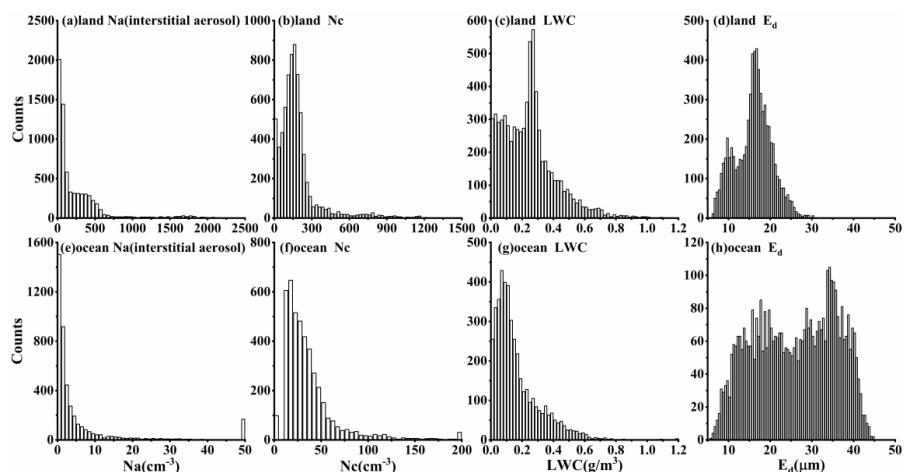
312 From 17:00 to 20:00, the descending and downdraft of the boundary layer increase  $N_a$  and  $N_c$   
313 in the lower cloud layer, and the number of large cloud droplets is less than 14:00 to 16:00. The  
314 aerosol retained above the top of the boundary layer provides sufficient cloud condensation nuclei  
315 for the middle layer and upper layer of the cloud. The  $N_a$  and  $N_c$  in this period are higher than those  
316 from 10:00 to 13:00, and the increase of cloud droplets with small particle-size is mainly due to the  
317 increase of  $N_a$  and  $N_c$ .

### 318 3.3 Influence of aerosols on microphysical quantities of stratified clouds

319 Previous studies have shown two sources of aerosols in Guangxi, namely the land and the



320 ocean, where air masses from land will bring higher aerosols. According to the classification of air  
321 mass sources, the frequency distributions of Na (interstitial aerosol), Nc, LWC and  $E_d$  under the  
322 influence of land and ocean air masses were obtained (Fig. 7).



323  
324 **Fig. 7** The distributions of cloud interstitial aerosol number concentration (a and e), cloud droplet number  
325 concentration (b and f), LWC (c and g) and cloud droplet effective diameter (d and h) under different air mass  
326 sources

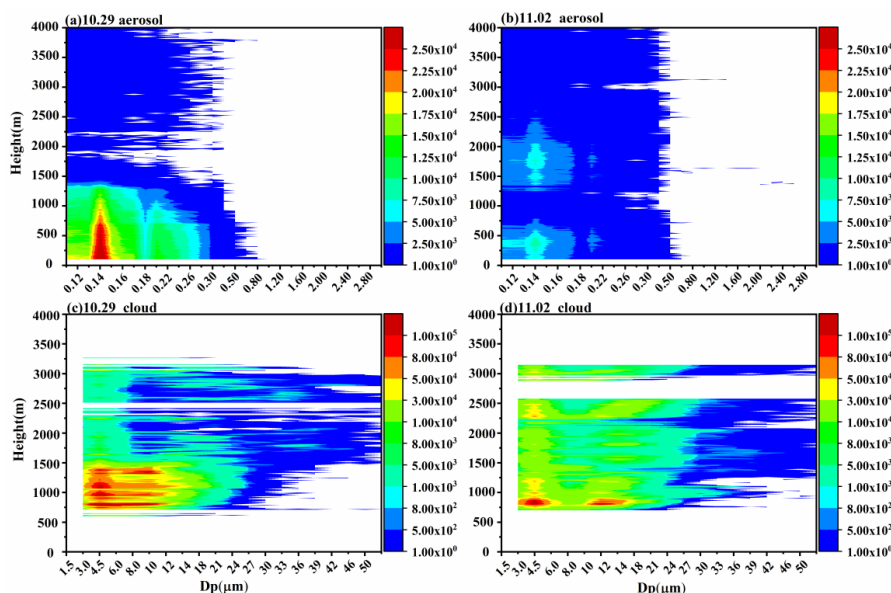
327 Under the influence of land air mass, Na (interstitial aerosol) was less than  $500 \text{ cm}^{-3}$ , Nc was  
328 high, and the frequency distribution of  $E_d$  was unimodal, mainly concentrated in the range of 16-18  
329  $\mu\text{m}$  (Fig. 7a). Under the influence of ocean air mass, Na (interstitial aerosol) was mainly less than  
330  $20 \text{ cm}^{-3}$ , and Nc was mostly distributed in the range of 10 to  $50 \text{ cm}^{-3}$ .  $E_d$  was significantly higher  
331 than that under the influence of land air mass.  $E_d$  presented a bimodal distribution with peak values  
332 of 17.75 and  $34.25 \mu\text{m}$  (Fig. 7b).

333 In addition to the influence of the air mass source, the vertical distribution of Na is also affected  
334 by PBL. We selected two aircraft observation data on October 29 and November 02 to analyze the  
335 influence of PBL on the cloud microphysical quantities. The observed cloud base height was lower  
336 than the PBL top's, and the cloud top height was  $> 1500 \text{ m}$ . The clouds crossed the PBL top, and the  
337 cloud thickness was similar (about 2500 m).

338 According to the vertical profiles of the aerosol number concentration spectrum (Fig. 8a-b),  
339 there were significant differences between the two Na profiles. For the height affected by PBL  
340 (below 1500 m), aerosol pollution occurred on October 29 ( $\text{Na} > 1000 \text{ cm}^{-3}$ ), and the atmosphere  
341 was relatively clean on November 2 ( $\text{Na} < 600 \text{ cm}^{-3}$ ). For the upper atmosphere (above 1500 m),



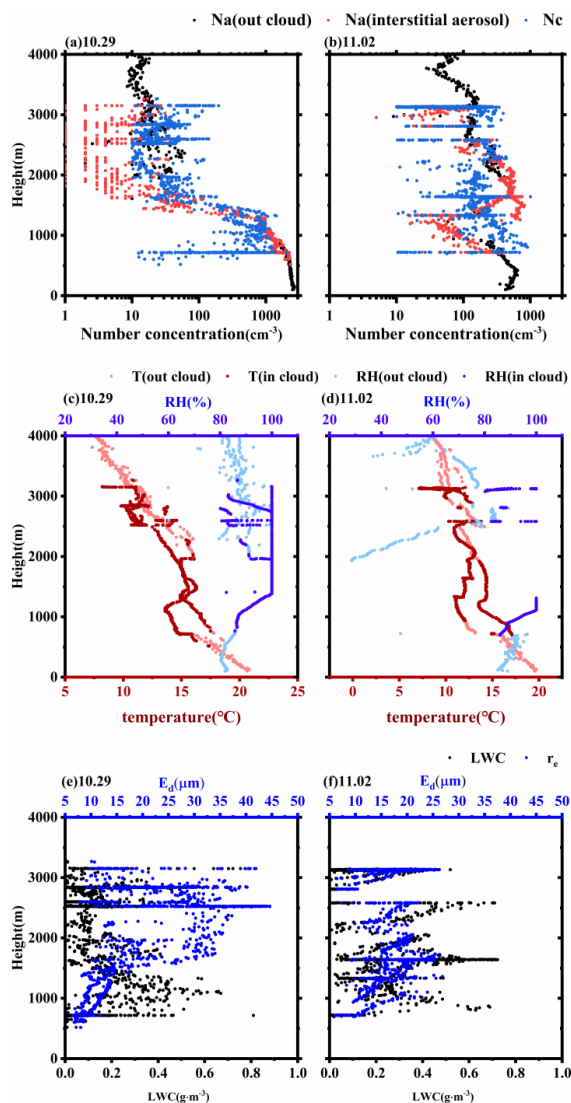
342 aerosol pollution ( $N_a < 200 \text{ cm}^{-3}$ ) occurred on November 2 compared to October 29 ( $N_a < 100 \text{ cm}^{-3}$ )  
343  $^3$ ).



344  
345 **Fig. 8** Vertical profiles of aerosol number concentration spectra (a and b) and cloud droplet number concentration  
346 spectra (c and d) on 29 October and 2 November

347 On October 29, the aerosol pollution in PBL was severe ( $N_a = 1331 \text{ cm}^{-3}$ ). The aerosol number  
348 concentration spectrum was bimodal, with peak diameters of 0.14 and 0.22  $\mu\text{m}$ . The atmosphere has  
349 sufficient cloud condensation nuclei, so the  $N_c$  is large ( $N_c = 460 \text{ cm}^{-3}$ ). It can be seen from the  
350 cloud droplet number concentration spectrum (Fig. 8c) that most of the cloud droplets were mainly  
351 concentrated in the range of 3–24  $\mu\text{m}$ . The average value of  $E_d$  was only 9.69  $\mu\text{m}$ , primarily because  
352 many cloud droplets compete for water vapor and it was difficult for them to grow into large cloud  
353 droplets. A strong inversion layer at 1500 m (Fig. 9c) made it difficult for aerosols to transmit  
354 upward.  $N_a$  above 1500 m was low, so  $N_c$  was also low, with an average value of only 35  $\mu\text{m}$ . Fig.  
355 8c showed that the concentration spectrum of cloud droplets presented a bimodal pattern, the  
356 number of cloud droplets with particle size in the range of 8.0–21  $\mu\text{m}$  decreased, and the particle  
357 size of cloud droplets was mainly distributed below 8  $\mu\text{m}$  and above 21  $\mu\text{m}$ . The average  $E_d$  reached  
358 25.28  $\mu\text{m}$ . These large particle-size cloud droplets may come from the collision and condensation  
359 growth of cloud droplets in the range of 8.0 to 21  $\mu\text{m}$ .





360

361

362

363

364

365

366

367

368

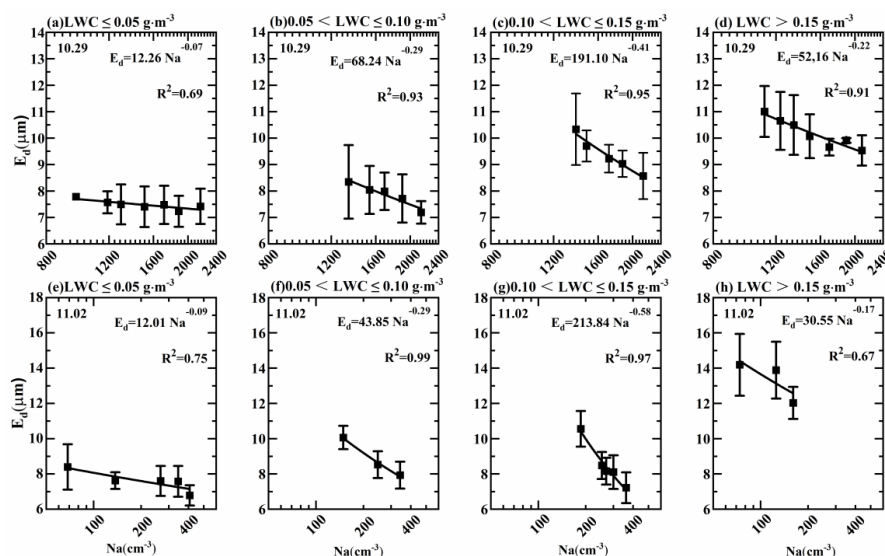
369

**Fig. 9** Vertical profiles of outside aerosol concentration, cloud intercloud aerosol concentration, cloud droplet concentration (a and b), temperature inside and outside the cloud, relative humidity inside and outside the cloud (c and d), LWC, and effective droplet diameters (e and f) on October 29 and November 2

On November 2, Na in PBL (mean  $405 \text{ cm}^{-3}$ ) was slightly higher than Na in the upper air (mean  $220 \text{ cm}^{-3}$ ). The aerosol spectral patterns were similar (Fig. 8b), both of which were bimodal and the peak particle sizes were  $0.14$  and  $0.22 \mu\text{m}$ , indicating that the aerosol pollution over this area may come from the transportation of near-surface aerosols in the surrounding areas of Guangxi. Nc in PBL (mean  $243 \text{ cm}^{-3}$ ) was slightly higher than Nc above PBL (mean  $124 \text{ cm}^{-3}$ ). The concentration spectra of cloud droplet numbers were all bimodal (Fig. 8d). A large number of small particle-size



370 cloud droplets in PBL hinder the growth of large cloud droplets, so the number of large cloud  
 371 droplets ( $D_p > 18 \mu\text{m}$ ) in PBL was lower than that in the upper air. And  $E_d$  in PBL (mean  $12.89 \mu\text{m}$ )  
 372 was lower than in the upper air (mean  $17.94 \mu\text{m}$ ). The inversion layer (about 750 m in thickness,  
 373 Fig. 9d) above the top of PBL enhanced the evaporation activity of cloud droplets, resulting in lower  
 374  $N_c$  at this height than  $N_c$  at other heights, and higher  $N_a$  (interstitial aerosol) than  $N_a$  (interstitial  
 375 aerosol) at other heights.



376  
 377 **Fig. 10** Correlation between aerosol number concentration and effective droplet diameter in the range of 0-0.05,  
 378 0.05-0.10, 0.10-0.15 and  $> 0.15 \text{ g}\cdot\text{m}^{-3}$  LWC (a-d are October 29, e-f are November 2,  $R^2$  is the correlation  
 379 coefficient)

380 To understand whether the relationship between aerosol and cloud in Guangxi is consistent  
 381 with the Twomey effect, we classified the in-cloud data below 1000 m on October 29 and November  
 382 2. We calculated the FIE index of LWC in different ranges (Fig. 10). The results showed that  $N_a$   
 383 and  $E_d$  were always negatively correlated regardless of low LWC condition or high LWC condition.  
 384 Therefore, the relationship between aerosol and stratocumulus in Guangxi is consistent with the  
 385 Twomey effect, and  $E_d$  decreases with the increase of  $N_a$ .

#### 386 4. Conclusion

387 This study provides the vertical profiles of stratocumulus microphysical quantities, number  
 388 concentration spectrum and meteorological elements over Guangxi in autumn using the aircraft  
 389 observation data of 9 sorties. The diurnal variations of cloud microphysical characteristics at



390 different altitudes are described, and the effects of air mass source and the boundary layer on cloud  
391 microphysical quantities are discussed. The results are as follows.

392 (1) Below 1500m in Guangxi, aerosol number concentration ( $N_a$ ) and cloud droplet  
393 concentration ( $N_c$ ) both decreased gradually with the increase of altitude. Aerosol is mainly  
394 concentrated near the ground, so  $N_c$  was larger, with an average value of  $407 \text{ cm}^{-3}$ . Between 1500  
395 m and 3300 m,  $N_a$  was low,  $N_c < 200 \text{ cm}^{-3}$ , and did not change with the height. With the increase in  
396 height, the effective diameter of the cloud droplet ( $E_d$ ) first increased, then remained unchanged,  
397 and finally increased.  $E_d$  of the cloud top was 2.75 times that of the cloud base. The inversion layer  
398 at the top of the boundary layer (PBL) hindered the increase in the cloud droplet particle size.  
399 Compared with other regions in China, LWC was high, with an average value of  $0.22 \text{ g}\cdot\text{m}^{-3}$ , and  
400 LWC variation was independent of height.

401 (2) The vertical distribution of microphysical quantities of stratospheric clouds in autumn in  
402 this region had noticeable diurnal variation, mainly influenced by the diurnal variation of the vertical  
403 distribution of aerosols. From 10:00 to 13:00, aerosols primarily concentrated in the low altitude,  
404 so there were more small particle-size cloud droplets in the lower cloud layer ( $N_c = 313 \text{ cm}^{-3}$ ,  $E_d =$   
405  $10.78 \mu\text{m}$ ). From 14:00 to 16:00, under the combined action of lifting the top of PBL and the updraft,  
406 the low-level aerosol diluted, decreasing the number of cloud droplets at the lower layer ( $N_c = 184$   
407  $\text{cm}^{-3}$ ). From 17:00 to 20:00, the descending and downdraft of PBL increased the number of small  
408 cloud droplets at the lower layer ( $E_d = 12.15 \mu\text{m}$ ). From 10:00 to 13:00,  $N_c$  in the middle and upper  
409 clouds was small, and the particle-size was large. From 14:00 to 20:00, the upward transport of  
410 aerosols near the surface and the formation of a high concentration aerosol layer (600-1300 m)  
411 increased the number of small particle-size cloud droplets in the middle and upper clouds.

412 (3) The source of air mass and PBL affected the distribution characteristics of cloud  
413 microphysical quantities by influencing  $N_a$ .  $N_c$  under the influence of the land air mass was 5.06  
414 times that of the ocean air mass, but  $E_d$  under the influence was 1.62 times that of the land air mass.  
415 When there was a high number concentration of aerosol below PBL, the cloud droplet number  
416 concentration spectrum was unimodal, and the cloud droplet size was concentrated below  $24 \mu\text{m}$ .  
417 Above PBL, the cloud droplet number concentration spectrum was bimodal, and the number of large  
418 particle-size cloud droplets (cloud droplet diameter  $>27 \mu\text{m}$ ) was more than that in PBL. The  
419 relationship between aerosol and cloud in the Guangxi region was consistent with the Twomey effect.



420  $E_d$  and  $N_a$  were negatively correlated in different LWC ranges, and FIE ranged from 0.07 to 0.58.

421

422 **Competing interests.** The contact authors have declared that none of the authors has any competing  
423 interests.

424

425 **Data availability.** All the aircraft data presented in this article can be accessed through  
426 <https://doi.org/10.5281/zenodo.13719678> (Wang, 2024). MERRA-2 data are available at  
427 <https://disc.gsfc.nasa.gov/daac-bin/FTPSubset2.pl> (Bosilovich et al., 2015).

428

429 **Author contributions.** **SL**, **HW**, **DZ**, and **MH** designed this study. **WZ**, **YD**, **ZZ**, and **PC**  
430 implemented the experiment and sample analysis. **SL** analysed the data and wrote the paper. **HW**,  
431 **DZ**, and **TZ**: Funding acquisition, Writing - review & editing. **YK** and **ZW**: Data curation. All co-  
432 authors proofread and commented on the paper.

433

434 **Acknowledgements.** The authors are grateful for the assistance of colleagues for sample  
435 collection. We would like to thank the GMAO for MERRA-2 data  
436 (<https://disc.gsfc.nasa.gov/datasets?keywords=MERRA-2>).

437

438 **Financial support.** This study was supported by the National Natural Science Foundation of  
439 China (42075084), the National Key Research and Development Program of China (Grant No.,  
440 2022YFC3701204) and the Natural Science Foundation of Jiangsu Province (BK20231300).

441

## 442 **References**

443 Albrecht B A. 1989. Aerosols, cloud microphysics, and fractional cloudiness [J]. *Science*, 245(4923):  
444 1227-1230. <https://doi.org/10.1126/science.245.4923.1227>

445 Almeida G, Brito J, Morales C, et al. 2014. Measured and modelled cloud condensation nuclei (CCN)  
446 concentration in São Paulo, Brazil: the importance of aerosol size-resolved chemical  
447 composition on CCN concentration prediction [J]. *Atmospheric Chemistry and Physics*,  
448 14(14): 7559-7572. <https://doi.org/10.5194/acp-14-7559-2014>

449 Betts A K. 2007. Coupling of water vapor convergence, clouds, precipitation, and land - surface



- 450 processes [J]. *Journal of Geophysical Research: Atmospheres*, 112(D10).  
451 <https://doi.org/10.1029/2006JD008191>
- 452 Bosilovich, M. G., Akella, S., Coy, L., Cullather, R., Draper, C., Gelaro, R., Kovach, R., Liu, Q.,  
453 Molod, A., Norris, P., Wargan, K., Chao, W., Reichle, R., Takacs, L., Vihliaev, Y., Bloom,  
454 S., Collow, A., Firth, S., Labow, G., Partyka, G., Pawson, S., Reale, O., Schubert, S. D.,  
455 Suarez, M., and Global Modeling and Assimilation Office (GMAO): MERRA-2, Greenbelt,  
456 MD, USA, Goddard Earth Sciences Data and Information Services Center (GES DISC),  
457 available at: <https://disc.gsfc.nasa.gov/daac-bin/FTPSubset2.pl> (last access: 7 January  
458 2024), 2015.
- 459 Che Y, Zhang J, Fang C, et al. 2021. Aerosol and cloud properties over a coastal area from aircraft  
460 observations in Zhejiang, China [J]. *Atmospheric Environment*, 267: 118771.  
461 <https://doi.org/10.1016/j.atmosenv.2021.118771>
- 462 Chen Y-C, Wang S-H, Min Q, et al. 2021. Aerosol impacts on warm-cloud microphysics and drizzle  
463 in a moderately polluted environment [J]. *Atmospheric Chemistry and Physics*, 21(6):  
464 4487-4502. <https://doi.org/10.5194/acp-21-4487-2021>
- 465 Collaud Coen M, Weingartner E, Apituley A, et al. 2010. Minimizing light absorption measurement  
466 artifacts of the Aethalometer: evaluation of five correction algorithms [J]. *Atmospheric  
467 Measurement Techniques*, 3(2): 457-474. <https://doi.org/10.5194/amt-3-457-2010>
- 468 de Boer G, Tripoli G J, Eloranta E W. 2008. Preliminary comparison of CloudSAT - derived  
469 microphysical quantities with ground - based measurements for mixed - phase cloud  
470 research in the Arctic [J]. *Journal of Geophysical Research: Atmospheres*, 113(D8).  
471 <https://doi.org/10.1029/2008JD010029>
- 472 Dusek U, Frank G, Hildebrandt L, et al. 2006. Size matters more than chemistry for cloud-nucleating  
473 ability of aerosol particles [J]. *Science*, 312(5778): 1375-1378.  
474 <https://doi.org/10.1126/science.1125261>
- 475 Feingold G, Eberhard W L, Veron D E, et al. 2003. First measurements of the Twomey indirect  
476 effect using ground - based remote sensors [J]. *Geophysical Research Letters*, 30(6).  
477 <https://doi.org/10.1029/2002GL016633>
- 478 Ferek R J, Hegg D A, Hobbs P V, et al. 1998. Measurements of ship - induced tracks in clouds off  
479 the Washington coast [J]. *Journal of Geophysical Research: Atmospheres*, 103(D18):



- 480 23199-23206. <https://doi.org/10.1029/98JD02121>
- 481 Ge J, Wang Z, Wang C, et al. 2021. Diurnal variations of global clouds observed from the CATS  
482 spaceborne lidar and their links to large-scale meteorological factors [J]. *Climate Dynamics*,  
483 57: 2637-2651.
- 484 Gunthe S, King S, Rose D, et al. 2009. Cloud condensation nuclei in pristine tropical rainforest air  
485 of Amazonia: size-resolved measurements and modeling of atmospheric aerosol  
486 composition and CCN activity [J]. *Atmospheric Chemistry and Physics*, 9(19): 7551-7575.  
487 <https://doi.org/10.5194/acp-9-7551-2009>
- 488 Han Q, Rossow W B, Lacis A A. 1994. Near-global survey of effective droplet radii in liquid water  
489 clouds using ISCCP data [J]. *Journal of Climate*, 7(4): 465-497.  
490 [https://doi.org/10.1175/1520-0442\(1994\)007%3C0465:NGSOED%3E2.0.CO;2](https://doi.org/10.1175/1520-0442(1994)007%3C0465:NGSOED%3E2.0.CO;2)
- 491 Harikishan G, Padmakumari B, Maheskumar R, et al. 2016. Aerosol indirect effects from ground -  
492 based retrievals over the rain shadow region in Indian subcontinent [J]. *Journal of*  
493 *Geophysical Research: Atmospheres*, 121(5): 2369-2382.  
494 <https://doi.org/10.1002/2015JD024577>
- 495 Jose S, Nair V S, Babu S S. 2020. Anthropogenic emissions from South Asia reverses the aerosol  
496 indirect effect over the northern Indian Ocean [J]. *Scientific reports*, 10(1): 18360.  
497 <https://doi.org/10.1038/s41598-020-74897-x>
- 498 Kennedy A D, Dong X, Xi B, et al. 2011. A Comparison of MERRA and NARR Reanalyses with  
499 the DOE ARM SGP Data [J]. *Journal of Climate*, 24(17): 4541-4557.
- 500 Kim B G, Schwartz S E, Miller M A, et al. 2003. Effective radius of cloud droplets by ground -  
501 based remote sensing: Relationship to aerosol [J]. *Journal of Geophysical Research:*  
502 *Atmospheres*, 108(D23). <https://doi.org/10.1029/2003JD003721>
- 503 King M D, Platnick S, Menzel W P, et al. 2013. Spatial and temporal distribution of clouds observed  
504 by MODIS onboard the Terra and Aqua satellites [J]. *IEEE transactions on geoscience and*  
505 *remote sensing*, 51(7): 3826-3852. <https://doi.org/10.1109/TGRS.2012.2227333>
- 506 Kleinman L I, Daum P H, Lee Y-N, et al. 2012. Aerosol concentration and size distribution measured  
507 below, in, and above cloud from the DOE G-1 during VOCALS-REx [J]. *Atmospheric*  
508 *Chemistry and Physics*, 12(1): 207-223. <https://doi.org/10.5194/acp-12-207-2012>
- 509 Koren I, Kaufman Y J, Rosenfeld D, et al. 2005. Aerosol invigoration and restructuring of Atlantic



- 510 convective clouds [J]. *Geophysical Research Letters*, 32(14).  
511 <https://doi.org/10.1029/2005GL023187>
- 512 Lance S, Nenes A, Rissman T A. 2004. Chemical and dynamical effects on cloud droplet number:  
513 Implications for estimates of the aerosol indirect effect [J]. *Journal of Geophysical*  
514 *Research: Atmospheres*, 109(D22). <https://doi.org/10.1029/2004JD004596>
- 515 Li J, Li P, Ren G, et al. 2019. Aircraft measurements of aerosol distribution, warm cloud  
516 microphysical properties, and their relationship over the Eastern Loess Plateau in China [J].  
517 *Tellus B: Chemical and Physical Meteorology*, 71(1): 1663994.  
518 <https://doi.org/10.1080/16000889.2019.1663994>
- 519 Li Z, Li R, Li B. 2003. Analyses on Vertical Microphysical Characteristics of Autumn Stratiform  
520 Cloud in Lanzhou Region [J]. *Plateau Meteorology*, 22(6): 583-589.  
521 <http://dx.chinadoi.cn/10.3321/j.issn:1000-0534.2003.06.008>
- 522 Liu S, Wang H, Zhao D, et al. 2024. Aircraft observations of aerosols and BC in autumn over  
523 Guangxi Province, China: Diurnal variation, vertical distribution and source appointment  
524 [J]. *Science of The Total Environment*, 906: 167550.  
525 <https://doi.org/10.1016/j.scitotenv.2023.167550>
- 526 Liu T, Liu Q, Chen Y, et al. 2020. Effect of aerosols on the macro-and micro-physical properties of  
527 warm clouds in the Beijing-Tianjin-Hebei region [J]. *Science of the total environment*, 720:  
528 137618. <https://doi.org/10.1016/j.scitotenv.2020.137618>
- 529 Lu C, Liu Y, Niu S. 2011. Examination of turbulent entrainment - mixing mechanisms using a  
530 combined approach [J]. *Journal of Geophysical Research: Atmospheres*, 116(D20).  
531 <https://doi.org/10.1029/2011JD015944>
- 532 Lu M L, Conant W C, Jonsson H H, et al. 2007. The marine stratus/stratocumulus experiment  
533 (MASE): Aerosol - cloud relationships in marine stratocumulus [J]. *Journal of Geophysical*  
534 *Research: Atmospheres*, 112(D10). <https://doi.org/10.1029/2006JD007985>
- 535 Lu Z, Liu X, Zhang Z, et al. 2018. Biomass smoke from southern Africa can significantly enhance  
536 the brightness of stratocumulus over the southeastern Atlantic Ocean [J]. *Proceedings of*  
537 *the National Academy of Sciences*, 115(12): 2924-2929.  
538 <https://doi.org/10.1073/pnas.1713703115>
- 539 McFarquhar G M, Bretherton C S, Marchand R, et al. 2021. Observations of clouds, aerosols,



540 precipitation, and surface radiation over the Southern Ocean: An overview of  
541 CAPRICORN, MARCUS, MICRE, and SOCRATES [J]. Bulletin of the American  
542 Meteorological Society, 102(4): E894-E928. <https://doi.org/10.1175/BAMS-D-20-0132.1>  
543 Miles N L, Verlinde J, Clothiaux E E. 2000. Cloud droplet size distributions in low-level stratiform  
544 clouds [J]. Journal of the atmospheric sciences, 57(2): 295-311.  
545 [https://doi.org/10.1175/1520-0469\(2000\)057%3C0295:CDSDIL%3E2.0.CO;2](https://doi.org/10.1175/1520-0469(2000)057%3C0295:CDSDIL%3E2.0.CO;2)  
546 Nakajima T Y, Uchiyama A, Takamura T, et al. 2005. Comparisons of warm cloud properties  
547 obtained from satellite, ground, and aircraft measurements during APEX intensive  
548 observation period in 2000 and 2001 [J]. Journal of the Meteorological Society of Japan.  
549 Ser. II, 83(6): 1085-1095. <https://doi.org/10.2151/jmsj.83.1085>  
550 Painemal D, Corral A F, Sorooshian A, et al. 2021. An overview of atmospheric features over the  
551 Western North Atlantic Ocean and North American East Coast—Part 2: Circulation,  
552 boundary layer, and clouds [J]. Journal of Geophysical Research: Atmospheres, 126(6):  
553 e2020JD033423.  
554 Painemal D, Kato S, Minnis P. 2014. Boundary layer regulation in the southeast Atlantic cloud  
555 microphysics during the biomass burning season as seen by the A - train satellite  
556 constellation [J]. Journal of Geophysical Research: Atmospheres, 119(19): 11,288-211,302.  
557 <https://doi.org/10.1002/2014JD022182>  
558 Pyrina M, Hatzianastassiou N, Matsoukas C, et al. 2015. Cloud effects on the solar and thermal  
559 radiation budgets of the Mediterranean basin [J]. Atmospheric Research, 152: 14-28.  
560 <https://doi.org/10.1016/j.atmosres.2013.11.009>  
561 Ramanathan V, Cess R, Harrison E, et al. 1989. Cloud-radiative forcing and climate: Results from  
562 the Earth Radiation Budget Experiment [J]. Science, 243(4887): 57-63.  
563 <https://doi.org/10.1126/science.243.4887.57>  
564 Rosenfeld D, Andreae M O, Asmi A, et al. 2014. Global observations of aerosol - cloud -  
565 precipitation - climate interactions [J]. Reviews of Geophysics, 52(4): 750-808.  
566 <https://doi.org/10.1002/2013RG000441>  
567 Strapp J W, Leaitch W, Liu P. 1992. Hydrated and dried aerosol-size-distribution measurements  
568 from the particle measuring systems FSSP-300 probe and the deiced PCASP-100X probe  
569 [J]. Journal of Atmospheric and Oceanic Technology, 9(5): 548-555.





- 570 [https://doi.org/10.1175/1520-0426\(1992\)009%3C0548:HADASD%3E2.0.CO;2](https://doi.org/10.1175/1520-0426(1992)009%3C0548:HADASD%3E2.0.CO;2)
- 571 Terai C, Bretherton C, Wood R, et al. 2014. Aircraft observations of aerosol, cloud, precipitation,  
572 and boundary layer properties in pockets of open cells over the southeast Pacific [J].  
573 Atmospheric Chemistry and Physics, 14(15): 8071-8088. [https://doi.org/10.5194/acp-14-](https://doi.org/10.5194/acp-14-8071-2014)  
574 8071-2014
- 575 Twomey S. 1977. The influence of pollution on the shortwave albedo of clouds [J]. Journal of the  
576 atmospheric sciences, 34(7): 1149-1152. [https://doi.org/10.1175/1520-](https://doi.org/10.1175/1520-0469(1977)034%3C1149:TIOPOT%3E2.0.CO;2)  
577 0469(1977)034%3C1149:TIOPOT%3E2.0.CO;2
- 578 Waliser D, Li J L, L'Ecuyer T, et al. 2011. The impact of precipitating ice and snow on the radiation  
579 balance in global climate models [J]. Geophysical Research Letters, 38(6).  
580 <https://doi.org/10.1029/2010GL046478>
- 581 Wang, H. 2024. Data for Aircraft observations of aerosol and microphysical quantities of  
582 stratocumulus in autumn over Guangxi Province, China: Diurnal variation, vertical  
583 distribution and aerosol-cloud relationship [Data set]. Zenodo.  
584 <https://doi.org/10.5281/zenodo.13719678>
- 585 Wang Y, Zheng X, Dong X, et al. 2020. Impacts of long-range transport of aerosols on marine-  
586 boundary-layer clouds in the eastern North Atlantic [J]. Atmospheric Chemistry and  
587 Physics, 20(23): 14741-14755. <https://doi.org/10.5194/acp-20-14741-2020>
- 588 Wehbe Y, Tessendorf S A, Weeks C, et al. 2021. Analysis of aerosol–cloud interactions and their  
589 implications for precipitation formation using aircraft observations over the United Arab  
590 Emirates [J]. Atmospheric Chemistry and Physics, 21(16): 12543-12560.  
591 <https://doi.org/10.5194/acp-21-12543-2021>
- 592 Wex H, McFiggans G, Henning S, et al. 2010. Influence of the external mixing state of atmospheric  
593 aerosol on derived CCN number concentrations [J]. Geophysical Research Letters, 37(10).
- 594 Wood R. 2012. Stratocumulus clouds [J]. Monthly Weather Review, 140(8): 2373-2423.  
595 <https://doi.org/10.1029/2010GL043337>
- 596 Yuan T, Li Z, Zhang R, et al. 2008. Increase of cloud droplet size with aerosol optical depth: An  
597 observation and modeling study [J]. Journal of Geophysical Research: Atmospheres,  
598 113(D4). <https://doi.org/10.1029/2007JD008632>
- 599 Zaveri R A, Wang J, Fan J, et al. 2022. Rapid growth of anthropogenic organic nanoparticles greatly



- 600           alters cloud life cycle in the Amazon rainforest [J]. *Science Advances*, 8(2): eabj0329.  
601           <https://doi.org/10.1126/sciadv.abj0329>
- 602   Zelinka M D, Andrews T, Forster P M, et al. 2014. Quantifying components of aerosol-cloud-  
603           radiation interactions in climate models [J]. *Journal of Geophysical Research: Atmospheres*,  
604           119(12): 7599-7615. <https://doi.org/10.1002/2014JD021710>
- 605   Zhang Q, Ma X, Tie X, et al. 2009. Vertical distributions of aerosols under different weather  
606           conditions: Analysis of in-situ aircraft measurements in Beijing, China [J]. *Atmospheric*  
607           *Environment*, 43(34): 5526-5535. <https://doi.org/10.1016/j.atmosenv.2009.05.037>
- 608   Zhang Q, Quan J, Tie X, et al. 2011. Impact of aerosol particles on cloud formation: Aircraft  
609           measurements in China [J]. *Atmospheric Environment*, 45(3): 665-672.  
610           <https://doi.org/10.1016/j.atmosenv.2010.10.025>
- 611   Zhao C, Klein S A, Xie S, et al. 2012. Aerosol first indirect effects on non - precipitating low -  
612           level liquid cloud properties as simulated by CAM5 at ARM sites [J]. *Geophysical*  
613           *Research Letters*, 39(8). <https://doi.org/10.1029/2012GL051213>
- 614   Zhao C, Qiu Y, Dong X, et al. 2018. Negative aerosol - cloud re relationship from aircraft  
615           observations over Hebei, China [J]. *Earth and Space Science*, 5(1): 19-29.  
616           <https://doi.org/10.1002/2017EA000346>
- 617   Zhao C, Zhao L, Dong X. 2019. A case study of stratus cloud properties using in situ aircraft  
618           observations over Huanghua, China [J]. *Atmosphere*, 10(1): 19.  
619           <https://doi.org/10.3390/atmos10010019>
- 620   Zhao Z, Mao J, Wang L, et al. 2011. In situ aircraft observations of one typical stratocumulus cloud  
621           process compared with the satellite measurements [J]. *Acta Meteorologica Sinica*, 69(03):  
622           521-527. <http://dx.doi.org/10.11676/qxxb2011.045>